Inorganic Chemistry
Article

Inorg. Chem. **2010**, *49*, 1733–1742 **1733**
DOI: 10.1021/ic902163w

Dihydrogen/Dihydride or Tetrahydride? An Experimental and Computational Investigation of Pincer Iridium Polyhydrides

Travis J. Hebden,[†] Karen I. Goldberg,[†] D. Michael Heinekey,*[,†] Xiawei Zhang,[‡] Thomas J. Emge,[‡] Alan S. Goldman,*[,‡] and Karsten Krogh-Jespersen*[,‡]

[†]*Department of Chemistry, University of Washington, Box 351700, Seattle, Washington 98195-1700 and* [‡]*Department of Chemistry and Chemical Biology, Rutgers, The State University of New Jersey, New Brunswick, New Jersey 08903*

Received November 2, 2009

The iridium pincer complexes (PCP)IrH_4 (**1**; PCP = [κ^3-1,3-$(CH_2P^tBu_2)_2C_6H_3$]) and (POCOP)IrH_4 (**2**; POCOP = [κ^3-1,3-$(OP^tBu_2)_2C_6H_3$]) have proven to be effective catalyst precursors for dehydrogenation of alkanes. The complex (POCOP)IrH_2 has also been applied successfully as a catalyst for release of H_2 from ammonia borane. Investigation of the "tetrahydride" forms of these complexes by solution NMR methods suggests their formulation as dihydrogen/dihydride species. This is in contrast to the solid state structure of **1**, determined by neutron diffraction (at 100 K), which indicates a compressed tetrahydride structure with only weak H−H interactions. Complex **1** ($C_{24}H_{47}IrP_2$) crystallizes in the space group $P4_2$, tetragonal, ($Z = 2$) with $a = 11.7006$ (19) Å, $c = 9.7008(27)$ Å, and $V = 1328.1(5)$ Å^3. Electronic structure calculations on **1** and **2** indicate that the global minima on the potential energy surfaces in the gas phase are tetrahydride structures; however, the dihydrogen/dihydride forms are only slightly higher in energy (1−3 kcal/mol). A dihydrogen/dihydride species is calculated to be the global minimum for **2** when in solution. The barriers to interconversion between the tetrahydride and dihydrogen/dihydride species are almost negligible.

Introduction

The class of compounds known as "pincer complexes" has become an extensively studied subfield of organometallic chemistry because of their wide range of catalytic activity.[1] Iridium complexes with tridentate pincer ligands featuring the "PCP" bonding motif have been employed as catalysts for both hydrogen transfer and acceptorless alkane dehydrogenation.[2] Both (PCP)IrH_2 (PCP = [κ^3-1,3-$(CH_2P^tBu_2)_2C_6H_3$]), and (POCOP)IrH_2 (POCOP = [κ^3-1,3-$(OP^tBu_2)_2C_6H_3$]) bind one molecule of H_2 reversibly to form their respective "tetrahydride" complexes: (PCP)IrH_4 (**1**) and (POCOP)IrH_4 (**2**), (Scheme 1). Recently, we have shown that the complex (POCOP)-IrH_2 is a highly effective catalyst for dehydrogenation of ammonia borane (AB).[3] When this reaction is carried out at ambient temperatures, the major Ir-containing species in solution is complex **2**. Dehydrogenation reactions of this type may prove useful in facilitating the development of hydrogen as a clean energy currency by allowing for chemical storage of H_2.[4]

Computational and experimental studies have been employed to elucidate the mechanism of transfer and acceptorless alkane dehydrogenation.[5] Strong support has been provided for a mechanism involving a three-coordinate Ir^I intermediate that undergoes oxidative addition of alkane C−H bonds. However, the Ir^I intermediate is not accessible

*To whom correspondence should be addressed. E-mail: heinekey@chem.washington.edu (D.M.H.), kroghjes@rutgers.edu (K.K.-J.), alan.goldman@rutgers.edu (A.S.G.).

(1) *The Chemistry of Pincer Compounds*; Morales-Morales, D., Jensen, C. M., Eds.; Elsevier: Amsterdam, The Netherlands, 2007.

(2) (a) Gupta, M.; Hagen, C.; Flesher, R. J.; Kaska, W. C.; Jensen, C. M. *Chem. Commun.* **1996**, 2083–2084. (b) Gupta, M.; Hagen, C.; Kaska, W. C.; Cramer, R. E.; Jensen, C. M. *J. Am. Chem. Soc.* **1997**, *119*, 840–841. (c) Liu, F.; Pak, E. B.; Singh, B.; Jensen, C. M.; Goldman, A. S. *J. Am. Chem. Soc.* **1999**, *121*, 4086–4087. (d) Zhang, X.; Fried, A.; Knapp, S.; Goldman, A. S. *Chem. Commun.* **2003**, 2060–2061. (e) Morales-Morales, D.; Redón, R.; Yung, C.; Jensen, C. M. *Inorg. Chim. Acta* **2004**, *357*, 2953–2956. (f) Göttker-Schnetmann, I.; White, P.; Brookhart, M. *J. Am. Chem. Soc.* **2004**, *126*, 1804–1811. (g) Göttker-Schnetmann, I.; White, P. S.; Brookhart, M. *Organometallics* **2004**, *23*, 1766–1776.

(3) (a) Denney, M. C.; Pons, V.; Hebden, T. J.; Heinekey, D. M.; Goldberg, K. I. *J. Am. Chem. Soc.* **2006**, *128*, 12048–12049. (b) Hebden, T. J.; Denney, M. C.; Pons, V.; Piccoli, P. M. B.; Koetzle, T. F.; Schultz, A. J.; Kaminsky, W.; Goldberg, K. I.; Heinekey, D. M. *J. Am. Chem. Soc.* **2008**, *130*, 10812–10820. (c) Dietrich, B. L.; Goldberg, K. I.; Heinekey, D. M.; Autrey, T.; Linehan, J. C. *Inorg. Chem.* **2008**, *47*, 8583–8585.

(4) (a) Marder, T. B. *Angew. Chem., Int. Ed. Engl.* **2007**, *46*, 8116–8118. (b) Stephens, F. H.; Pons, V.; Baker, R. T. *Dalton Trans.* **2007**, 2613–2626. (c) Hamilton, C. W.; Baker, R. T.; Staubitz, A.; Manners, I. *Chem. Soc. Rev.* **2009**, *38*, 279–293.

(5) (a) Jensen, C. M. *Chem. Commun.* **1999**, 2443–2449. (b) Krogh-Jespersen, K.; Czerw, M.; Summa, N.; Renkema, K. B.; Achord, P. D.; Goldman, A. S. *J. Am. Chem. Soc.* **2002**, *124*, 11404–11416. (c) Renkema, K. B.; Kissin, Y. V.; Goldman, A. S. *J. Am. Chem. Soc.* **2003**, *125*, 7770–7771. (d) Göttker-Schnetmann, I.; Brookhart, M. *J. Am. Chem. Soc.* **2004**, *126*, 9330–9338. (e) Zhu, K.; Achord, P. D.; Zhang, X.; Krogh-Jespersen, K.; Goldman, A. S. *J. Am. Chem. Soc.* **2004**, *126*, 13044–13053.

Published on Web 01/22/2010

Scheme 1

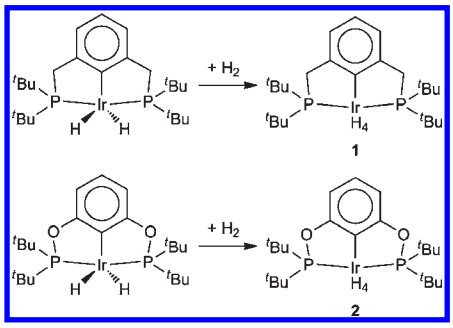

under the conditions employed in AB dehydrogenation, indicating that alkane and AB dehydrogenation reactions occur by different mechanisms. Accordingly, a computational study by Paul and Musgrave suggests a novel concerted activation of both the B−H and the N−H bonds of AB by (POCOP)IrH_2 to yield a tetrahydride.[6] In this case, the tetrahydride species may be a part of the catalytic cycle, whereas in the case of alkane dehydrogenation it plays the role of a catalyst precursor.

Calculations involving transition metal polyhydrides are often confounded by the fact that several plausible structures are calculated to have similar energies. Interpretation of NMR observations is often complicated by rapid H atom permutation. In our view, a full understanding of the molecular structures and properties of these complexes can only be obtained through a combination of experiment and computation.

The present work is concerned with the structures of **1** and **2** in solution, in the solid state, and in the gas phase. Solution state data have been obtained using NMR and IR spectroscopies. Solid state data for **1** has been obtained by neutron diffraction. Structures for complexes **1** and **2** have been calculated in the idealized gas phase and in simulated nonpolar and polar solvents.

Results

Characterization of (PCP)IrH_4 by NMR Spectroscopy. Addition of D_2 gas to an NMR tube containing a degassed solution of (PCP)IrH_4 allowed the isotopomers of **1** to be observed by NMR spectroscopy. A statistical distribution of isotopes in the hydridic positions was achieved in minutes at room temperature by gently shaking the sample tube. The isotope effects on the ^1H chemical shifts in this complex are small (less than 10 ppb per deuteron), making it impossible to distinguish individual isotopomers. Adequate control over the total % D bound to Ir was achieved by repeated cycles of freezing the sample, evacuating the headspace, and repressurizing with D_2 gas. Observation of a single isotopomer, **1-d_3**, was achieved by adjusting the total % D bound to Ir to 98%.[7] Formation of (PCP)IrH_2 by loss of H_2 from complex **1** requires more vigorous conditions than the analogous reaction for **2**.[2b,f] This difference did not affect the ability to control the level of deuteration.

Variable temperature NMR data was collected for **1** at 180−298 K (Table 1). The hydridic resonance was observed as a triplet in the ^1H NMR spectra at all temperatures down to 180 K, where the resonance was too broad for coupling to be observed. More detailed tables can be found in Supporting Information.

Table 1. Variable Temperature $^1H\{^{31}P\}$ NMR Data for **1**, **1-d_3**, **2**, and **2-d_3** in THF-d_8

	1	**1-d_3**	**2**	**2-d_3**[a]
temperature (K)	δ (ppm)	J_{obs} (Hz)	δ (ppm)	J_{obs} (Hz)
318		3.56 ± 0.09		
308		3.61 ± 0.07		
298	−9.42	3.52 ± 0.09	−8.60	
293			−8.60	
287		3.60 ± 0.07		
283			−8.61	
273			−8.62	4.38 ± 0.12
270				4.39 ± 0.02
263			−8.63	
260				4.33 ± 0.07
250				4.40 ± 0.03
243			−8.66	
240				4.39 ± 0.02
230	−9.52			
223			−8.68	
220	−9.54			
210	−9.56			
203			−8.71	
200	−9.58			
190	−9.58			
183			−8.74	
180	−9.60			

[a] Only five of the expected seven lines were resolved in these spectra.

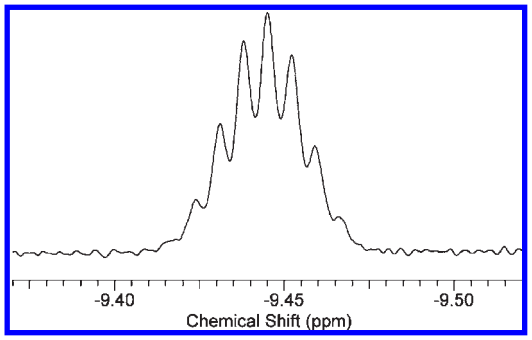

Figure 1. Partial (hydride region) $^1H\{^{31}P\}$ NMR spectrum of **1-d_3** (298 K, THF-d_8, 500 MHz). This sample contains 2% residual H atoms in the hydridic sites.

A minimum relaxation time (T_1(min)) of the hydride resonance of complex **1** has been reported previously.[8] This parameter was redetermined; the T_1(min) for **1** was observed at 220 K as 130 msec in toluene-d_8 (500 MHz) and at 210 K as 130 msec in THF-d_8 (500 MHz). H−D coupling was observed for **1-d_3** in THF-d_8 at temperatures ranging from 287−318 K, with J_{obs} = 3.55 ± 0.13 Hz, as summarized in Table 1. (Several individual H−D interactions contribute to an average observed coupling. Analysis of this coupling appears in the Discussion section.) Above 318 K the hydridic resonance broadens significantly, preventing observation of coupling. This coupling was also observed in toluene-d_8 at 298 K with J_{obs} = 3.52 ± 0.10 Hz. A representative example of the observed resonance for **1-d_3** is shown in Figure 1.

(6) Paul, A.; Musgrave, C. B. *Angew. Chem., Int. Ed. Engl.* **2007**, *46*, 8153–8156.

(7) For 2.0% protonation of the hydridic sites, the populations of the species **[Ir]H_4**, **[Ir]H_3D**, **[Ir]H_2D_2**, **[Ir]HD_3**, and **[Ir]D_4** are 0.0, 0.0, 0.2, 7.5, and 92.2% respectively. The observed resonance results from 6 and 94% of **[Ir]H_2D_2** and **[Ir]HD_3** respectively.

(8) Gupta, M. *Catalytic Dehydrogenation of Saturated Hydrocarbons and Furan by a Novel Iridium P-C-P Pincer Complex*. Ph.D. Thesis, University of Hawaii, Manoa, HI, December **1997**.

Table 2. Observed Coupling of **2-d_3** in Various Solvents at 273 K

solvent	% H	J_{obs} (Hz)
THF-d_8	1.2	4.40 ± 0.06
toluene-d_8	1.8	4.30 ± 0.11
CD_2Cl_2	(2)[a]	4.66 ± 0.04
MeCy-d_{14}	1.9	4.10 ± 0.24
C_6D_5F	1.6	4.58 ± 0.15
Acetone-d_6	0.8	4.47 ± 0.18

[a] Decomposition of **2** in CD_2Cl_2 led to formation of (POCOP)IrDCl and other products. Overlapping signals in the aryl region of the $^1H\{^{31}P\}$ NMR spectrum prevented precise integration of the hydridic resonance. The signal line shape indicated that an approximate residual H of 2% or less was present in this sample.

Characterization of (POCOP)IrH_4 by NMR Spectroscopy. All experiments (measurement of T_1(min) for the hydridic resonance of **2** and observation of coupling in **2-d_3**) were carried out in a similar manner to those for **1**. A single hydridic resonance was observed at all temperatures (183−298 K) corresponding to four hydrogen atoms bound to iridium. The T_1(min) for **2** was observed at 220 K as 110 msec in toluene-d_8 (500 MHz) and at 210 K as 110 msec in THF-d_8 (500 MHz). The variable temperature ^1H NMR data of the hydridic resonance is summarized in Table 1. Above 283 K this resonance was a broad singlet. From 283 K through 223 K, coupling to phosphorus atoms was resolved; however, below 223 K this coupling was no longer observed. In the range for which coupling to phosphorus was observed, the $^1H\{^{31}P\}$ NMR spectra were recorded (see Supporting Information) resulting in a singlet hydridic resonance at all temperatures. Coupling in the $^1H\{^{31}P\}$ NMR spectra of **2-d_3** was observed at various temperatures in THF-d_8 solution (Table 1) and at 273 K in various solvents (Table 2).

Observation of *cis* and *trans* Scalar Coupling in (POCOP)-IrH_3^- Na^+. The previously reported complex[2g] (POCOP)-IrH_3^- Na^+ was observed to exhibit reasonable absolute values for *cis* and *trans* H−H scalar couplings for application to the tetrahydride complexes. The reported absolute value of $^2J_{cis\mathrm{HH}}$ = 4.8 Hz was confirmed (THF-d_8, 298 K), which would correspond to $^2J_{cis\mathrm{HD}}$ = 0.7 Hz. (The complex (POCOP)IrH_3^- Na^+ is static on the NMR time scale, allowing for direct observation of the relevant couplings.) The *trans* coupling was obtained in a manner similar to observation of HD coupling in complexes **1-d_3** and **2-d_3**. The observed sample contained 98% deuterium in the hydridic positions. The $^2J_{trans\mathrm{HD}}$ was too small to be directly observed; however, fitting the line shape of the resulting spectrum is consistent with $^2J_{trans\mathrm{HD}} \approx 0.7$ Hz.[9]

Characterization of (PCP)IrH_4 by IR Spectroscopy. Complex **1** was investigated using IR spectroscopy in both solution and the solid state. The thermal stability of **1** in the absence of H_2 gas allowed IR spectra of reasonable quality to be obtained. The spectral region attributed to Ir−H fundamental stretching modes is shown in Figure 2; three peaks are clearly identifiable. The solid and solution state spectra are nearly identical and are composed of an intense broad feature at low frequency, a medium intensity absorption band at higher frequency, and weak absorption at even higher frequency. Using a sample of **1-d_4** with complete deuteration of the hydridic positions led to disappearance of these signals and the appearance of new absorptions at lower energy.

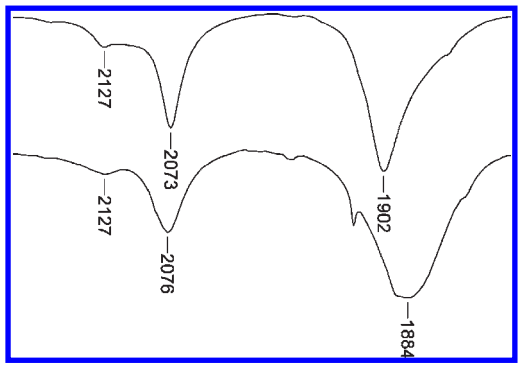

Figure 2. Infrared spectra of **1** in cyclopentane solution (bottom) and as a solid in a KBr pellet (top) showing the region containing peaks attributed to Ir−H stretching modes. Peak labels are in units of wavenumbers (cm^{-1}). Full spectra can be found in the Supporting Information.

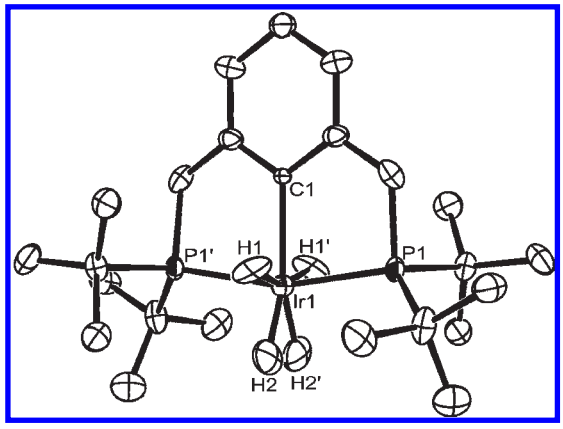

Figure 3. ORTEP of complex **1** determined by neutron diffraction at 100 K. Hydrogen atoms other than those in the coordination sphere of the Ir atom have been omitted for clarity. Ellipsoids are shown at 50% probability.

Solid State Structure of Complex 1. The structure of complex **1** has been determined by neutron diffraction. The data collection and refinement parameters are summarized in the Supporting Information. Details of the structure determination are given in the Experimental Section. An Oak Ridge thermal ellipsoid plot (ORTEP) diagram of the structure is shown in Figure 3. A summary of crystallographic data for **1** is presented in Table 3. Selected bond distances and angles are shown in Table 4.

Computational Investigations on 1 and 2. Several density functional theory (DFT)[10] functionals were tested on potential structures for **1** and **2** (Chart 1) and their energetics. Hybrid functionals, which include some Hartree−Fock (exact) exchange, appeared to perform better than pure exchange-correlation functionals.[11] In particular, the robust B3LYP set of functionals,[12] which have shown good performance in computational studies of

(9) Budzelaar, P. H. M. *gNMR: NMR Simulation Program*, version 5.0.6.0; IvorySoft: Denver, CO, 2006.

(10) Parr, R. G.; Yang, W. *Density-Functional Theory of Atoms and Molecules*; University Press: Oxford, 1989.

(11) Sousa, S. F.; Fernandes, P. A.; Ramos, M. J. *J. Phys. Chem. A* **2007**, *111*, 10439–10452.

(12) (a) Becke, A. D. *J. Chem. Phys.* **1993**, *98*, 5648–5652. (b) Lee, C.; Yang, W.; Parr, R. G. *Phys. Rev. B.* **1988**, *37*, 785–789.

Table 3. Crystallographic Data for **1**

parameter	**1**
formula	$C_{24}H_{47}IrP_2$
fw (g mol^{-1})	589.79
space group	$P4_2$ (No. 77)
a (Å)	11.7006(19)
c (Å)	9.7008(27)
V (Å^3)	1328.1(5)
Z	2
temp. (K)	100(1)
radiation	neutrons
data collection technique	time-of-flight Laue
D_{calc} (g cm^{-3})	1.575
$\mu(\lambda)$ (cm^{-1})	1.757 + 1.785 λ
$R(F^2)^a$	0.190
$R_w(F^2)^b$	0.137

^{a} $R(F^2) = \sum[F_o^2 - F_c^2]/\sum F_o^2$. ^{b} $R_w(F^2) = \{\sum w(F_o^2 - F_c^2)^2/\sum w(F_o^2)^2\}^{0.5}$.

Table 4. Selected Bond Distances and Angles for **1**

atoms	distance (Å)
Ir1−H1	1.697(8)
Ir1−H2	1.546(11)
Ir1−P1	2.341(5)
Ir1−C1	2.125(7)
H1−H2	1.919(16)
H2−H2′	1.488(23)
atoms	**angle (deg)**
C1−Ir1−H1	78.87(34)
H1−Ir1−H2	72.4(6)
H2−Ir1−H2′	57.5(9)
C1−Ir1−P1	81.81(18)

metal-polyhydrides by others,[13] appeared to yield results on **1** and **2** compatible with several experimental observations; therefore, only these computational results will be featured here. Some structural and energetic data obtained with other functionals are available in the Supporting Information.

Relative energies of structural minima for **1** and **2**, the transition states that interconnect them, and key H−H distances (Chart 1) are shown in Table 5.[14] Minima corresponding to the bis-(dihydrogen) structures **1D** or **2D** could not be located on the potential energy surfaces. Unconstrained geometry optimizations invariably produced the tetrahydride species **1A** or **2A**; constrained optimizations with fixed H−H distances of 0.9 Å lead to transition state (TS) structures, which lay approximately 25 kcal/mol above the tetrahydride structures. The geometries of **1** and **2** were reoptimized with solvent (cyclohexane or THF) represented by a continuum dielectric model. A summary of the structural and energetic results obtained from these simulated solution phase calculations is presented in Table 6.

The vibrational frequencies for **1** were evaluated in the harmonic oscillator approximation for the structures optimized in cyclohexane solvent. Unscaled calculated

Chart 1. Potential Structures (**A**−**D**) and Key H−H Distances (r_1, r_2, r_3) for Polyhydrides **1** and **2**

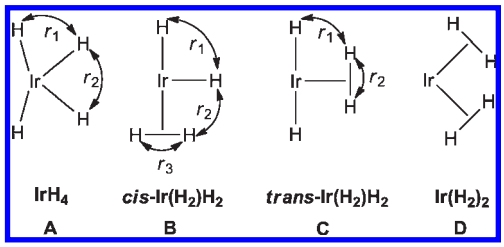

frequencies for the four Ir−H stretching modes along with the predicted (absolute and relative) IR intensities are tabulated in the Supporting Information. A graphical representation of selected species is shown in Figure 4.

An attempt to assess the importance of anharmonicity was made by optimizing the isomers of **1** with phosphino ^{t}Bu groups replaced by hydrogens ((^{H}PCP)IrH$_4$, **1-H-A**, **B**,**C**) in model cyclohexane solvent, followed by evaluation of vibrational frequencies in the harmonic and anharmonic approximations (Table 7). An approximate set of anharmonic Ir−H frequencies can then be constructed for **1**, if we assume that the anharmonicity corrections for frequencies of **1-H** and **1** are the same (Table 7).

Discussion

Historically, hydrogen addition to a metal complex was assumed to result in oxidative addition to form the corresponding dihydride complex. The seminal work of Kubas,[15] however, revealed that the hydrogen molecule could bind to a metal atom in a side-on fashion, keeping the H−H bond largely intact.[16] After this discovery, a metal bound to two or more hydrogen atoms was cast as either a "classical" dihydride complex or a "non-classical" dihydrogen complex. Reinvestigation of polyhydride complexes, which had previously been assigned unusually high oxidation states, led in some cases to reformulation with at least one dihydrogen ligand. As the body of data concerning "non-classical" hydrogen complexes grew, it became obvious that many of these complexes did not fit neatly into either of the categories available, leading to the creation of new descriptors such as "elongated dihydrogen" and "compressed dihydride". By now it is clear that the degree of H_2 bond activation can exist along a broad continuum from a nearly fully intact H−H bond to a classical dihydride in which oxidative addition of the H_2 bond has gone to completion (Chart 2).[17]

Characterization of compounds in which only two hydrogen atoms are in question has become relatively straightforward; compounds containing three or more hydrogen atoms remain more challenging. These complexes are often highly dynamic, and the observed NMR signal represents a population weighted average of all of the hydridic positions present in the molecule.

NMR Studies. The ^{1}H{^{31}P} NMR spectra of **1** and **2** exhibit a single hydridic resonance at all observation temperatures (180−318 K for **1**, 183−298 K for **2**)

(13) (a) Webster, C. E.; Singleton, D. A.; Szymanski, M. J.; Hall, M. B.; Zhao, C.; Jia, G.; Lin, Z. *J. Am. Chem. Soc.* **2001**, *123*, 9822–9829. (b) Gelabert, R.; Moreno, M.; Lluch, J. M.; Lledós, A.; Pons, V.; Heinekey, D. M. *J. Am. Chem. Soc.* **2004**, *126*, 8813–8822. (c) Gelabert, R.; Moreno, M.; Lluch, J. M.; Lledós, A. *J. Am. Chem. Soc.* **1997**, *119*, 9840–9847.

(14) These values were also calculated for thermodynamic conditions of T = 100 K and P = 1 atm, but did not display notable differences. This data can be found in the Supporting Information.

(15) Kubas, G. J.; Ryan, R. R.; Swanson, B. I.; Vergamini, P. J.; Wasserman, H. J. *J. Am. Chem. Soc.* **1984**, *106*, 451–452.

(16) Kubas, G. J. *Metal Dihydrogen and σ-Bond Complexes*; Kluwer Academic/Plenum Publishers: New York, 2001.

(17) Kubas, G. *J. Chem. Rev.* **2007**, *107*, 4152–4205.

Table 5. Calculated Energetics (kcal/mol) and H−H Distances (Chart 1, Å) for **1** and **2** in Idealized Gas-Phase[a]

species	ΔE	ΔH	ΔG	ΔS	r_1	r_2	r_3
$(PCP)IrH_4$, **1A**	0.00	0.00	0.00	0.00	1.866	1.691	
trans-$(PCP)Ir(H_2)H_2$, **1C**	0.62	0.89	1.41	−1.76	2.141	0.932	
cis-$(PCP)Ir(H_2)H_2$, **1B**	2.19	2.96	3.14	−0.59	2.170	2.101	0.890
TS **1A** ↔ **1C**	1.39	0.40	1.40	−3.37	2.030	1.177	
TS **1A** ↔ **1B**	3.31	2.39	2.72	−1.11	2.090	1.958	1.161
$(POCOP)IrH_4$, **2A**	0.00	0.00	0.00	0.00	1.842	1.710	
trans-$(POCOP)Ir(H_2)H_2$, **2C**	0.71	0.89	0.93	−0.12	2.117	0.919	
cis-$(POCOP)Ir(H_2)H_2$, **2B**	0.73	1.35	0.29	3.58	2.143	2.099	0.874
TS **2A** ↔ **2C**	1.47	0.49	0.78	−1.00	2.007	1.187	
TS **2A** ↔ **2B**	2.57	1.81	1.49	1.07	2.046	1.942	1.209

[a] Thermodynamic conditions: $T = 298$ K, $P = 1$ atm.

Table 6. Calculated Free Energies (kcal/mol) and H−H Distances (Chart 1, Å) for **1** and **2** in Simulated Cyclohexane and THF Solutions

	cyclohexane				THF			
species	ΔG	r_1	r_2	r_3	ΔG	r_1	r_2	r_3
$(PCP)IrH_4$, **1A**	0.00	1.860	1.719		0.00	1.857	1.741	
trans-$(PCP)Ir(H_2)H_2$, **1C**	1.55	2.148	0.917		1.67	2.144	0.919	
cis-$(PCP)Ir(H_2)H_2$, **1B**	2.47	2.179	2.125	0.879	1.76	2.186	2.146	0.873
$(POCOP)IrH_4$, **2A**	0.00	1.835	1.740		0.00	1.829	1.756	
trans-$(POCOP)Ir(H_2)H_2$, **2C**	0.95	2.120	0.910		0.80	2.122	0.903	
cis-$(POCOP)Ir(H_2)H_2$, **2B**	−0.48	2.150	2.116	0.866	−1.21	2.157	2.131	0.859

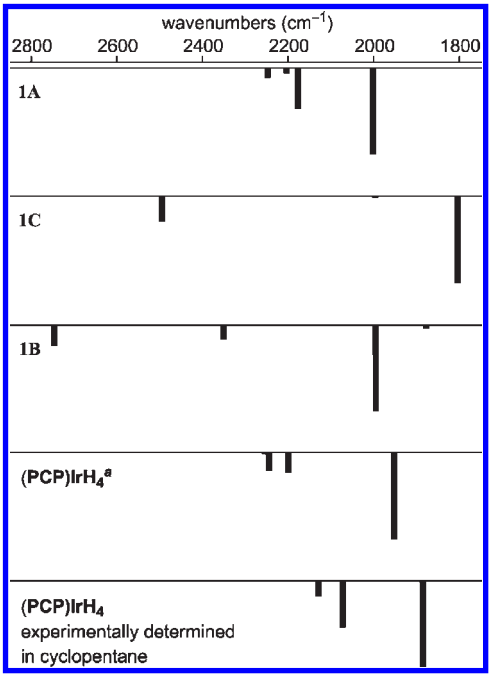

Figure 4. Stick diagram comparing the location and intensities of calculated and experimental Ir−H stretching bands. Sticks are displayed using normalized intensities relative to the most intense band in each representation. [a] All Ir−H bond distances and C(PCP)−Ir−H bond angles are fixed at the values derived from neutron scattering.

corresponding to four hydrogen atoms bound to iridium, indicating that H atom permutation is rapid on the NMR time scale. The pincer ligands employed in this study bind in a meridional orientation, enforcing a perpendicular meridional arrangement of hydrogen atoms about the iridium centers. There are several plausible structures for complexes **1** and **2** as illustrated in Chart 1.

The minimum relaxation times (T_1(min)) for the hydridic resonances were found to be 130 msec in complex **1** and 110 msec in complex **2** (210−220 K). Utilizing the methods described by Halpern and co-workers,[18] this data can be analyzed in terms of the possible structures for **1** and **2** depicted in Chart 1. This analysis was carried out using heavy atom locations determined by neutron diffraction analysis for **1** and an average Ir−H distance. The positions of the H atoms relative to each other in a plane orthogonal to that defined by the pincer ligand were varied according to the structure being considered.

An averaged relaxation rate for all individual H atom positions must be considered to calculate an expected T_1 value. Assuming a tetrahydride structure (**A**) leads to a calculated T_1 value of 110−130 msec, corresponding to $r_{HH} = 1.55-1.60$ Å. Although short, these distances are acceptable for a tetrahydride structure. Structure **B** may be considered with the same initial Ir−P and Ir−H assumptions made for structure **A**. A T_1 value of 110−130 msec can be calculated for an assumed octahedral geometry with $r_{HH} = 1.33-1.39$ Å in the dihydrogen ligand. This analysis assumes that the hydride and dihydrogen ligands are at angles of 90° to one another around the Ir center. A similar analysis for structure **C** results in a calculated T_1 of 127 msec or less for all values of r_{HH}. (A T_1 of 127 msec is calculated for r_{HH} values of 1.57−1.59 Å.). In contrast, the bis-(dihydrogen) structure (**D**) cannot give rise to the observed T_1(min) data without the assumption of unreasonably long H−H distances. This analysis simply indicates that structures **A**, **B**, and **C** are not distinguishable using relaxation data alone; however, the possibility of **D** may be excluded.

Calculating a T_1 using core atom positions obtained from neutron diffraction data of **1** results in a value of 173 msec. When H atoms in the ^{t}Bu groups of the ligands are included, the expected value drops to 136 msec. It is noteworthy that the remote H atoms on the ligand have a

(18) Desrosiers, P. J.; Cai, L.; Lin, Z.; Richards, R.; Halpern, J. *J. Am. Chem. Soc.* **1991**, *113*, 4173–4184.

Table 7. Calculated Ir−H Vibrational Frequencies for **1** and **1-H** in Model Cyclohexane Solvent[a]

species	ν_4	ν_3	ν_2	ν_1
(^{H}PCP)IrH$_4$, **1−H-A**	2170, *2074*	2161, *2075*	2116, *2041*	1900, *1823*
trans-(^{H}PCP)Ir(H$_2$)H$_2$, **1−H-C**	2533, *2194*	2074, *1970*	1915, *1825*	1754, *1670*
cis-(^{H}PCP)Ir(H$_2$)H$_2$, **1−H-B**	2698, *2129*	2244, *2150*	2010, *1935*	1778, *1668*
(PCP)IrH$_4$, **1A**[b]	2190, *2094*	2158, *2072*	2122, *2047*	1947, *1870*
trans-(PCP)Ir(H$_2$)H$_2$, **1C**[b]	2440, *2101*	2126, *2022*	1940, *1850*	1797, *1713*
cis-(PCP)Ir(H$_2$)H$_2$, **1B**[b]	2689, *2120*	2292, *2198*	1945, *1870*	1834, *1724*
experiment, **1**[c]	2127		2076	1884

[a] For each mode, both the harmonic and anharmonic (in italics) frequencies are given. [b] Anharmonic frequency obtained assuming that the anharmonicity corrections for frequencies in **1-H** and **1** are the same. [c] In cyclopentane.

Chart 2. Varying Degrees of H−H Bond Elongation in Transition Metal Complexes

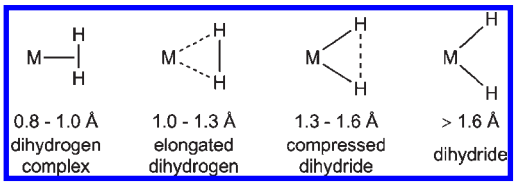

significant effect on T_1, emphasizing that the accuracy of the predicted T_1 values is dependent on knowledge of these H atom positions.

The relaxation data is consistent with structures **A**, **B**, and **C**. Likewise, the observed solution T_1(min) for complex **1** is consistent with the expected T_1 calculated using neutron diffraction data within reasonable error. These results are similar to the case of hydridotris(pyrazolyl)-borato iridium(V) tetrahydride,[13a,19] in which experimental T_1 data and computational studies were unable to distinguish the ground state structure as either a tetrahydride or a dihydrogen/dihydride.[20]

Observation of H−D coupling (J_{HD}) allows an independent experimental method of structure elucidation in polyhydride complexes and in principle allows for the unambiguous detection of a dihydrogen ligand.[13b] In complexes **1** and **2**, insignificant chemical shift isotope effects complicate direct observation of J_{HD} in moderately deuterated complexes. (The subspectra of the isotopomers overlap significantly.) This problem can be overcome by preparation of samples with a high degree of deuteration, which allows for observation of [Ir]HD$_3$ almost exclusively. A representative hydride region of the resulting ^{1}H{^{31}P} NMR spectrum for complex **1** is shown in Figure 1.

In the case of *trans*-Ir(H$_2$)H$_2$ (**C**) complexes, the observed H−D coupling (J_{obs}) represents an average of three different types of H−D interactions (illustrated in Chart 3, top) and can be interpreted using the equation

$$J_{obs} = \frac{^1J_{HD} + 4^2J^*_{HD} + ^2J_{HD}}{6} \quad (1)$$

where (as described by Girolami and co-workers for osmium dihydrogen/dihydride complexes[21]) $^1J_{HD}$ is the coupling in the bound dihydrogen ligand, $^2J_{HD}$ represents the two bond coupling between hydride ligands, and the coupling between a hydride and an adjacent dihydrogen moiety is designated as $^2J^*_{HD}$. In the case of *cis*-Ir(H$_2$)H$_2$ (**B**), J_{obs} is an average of four types of H−D interactions (illustrated in Chart 3, middle) and can be interpreted using the equation

Chart 3. Individual H−D Couplings Which Contribute to J_{obs}

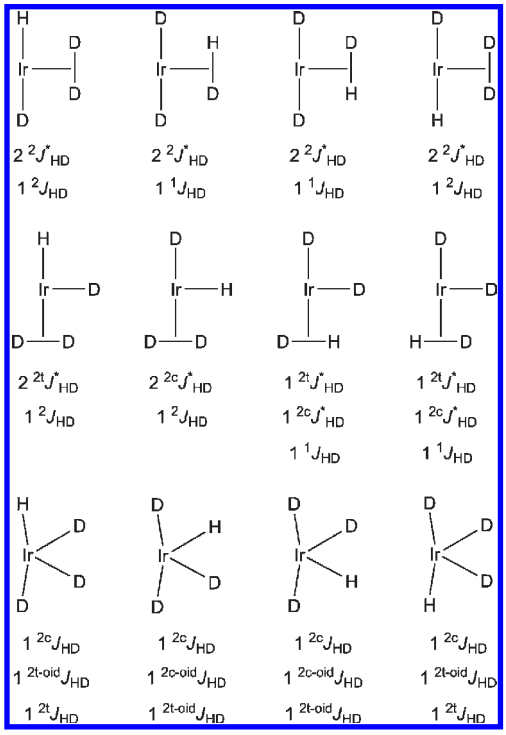

$$J_{obs} = \frac{^1J_{HD} + 2^{2c}J^*_{HD} + 2^{2t}J^*_{HD} + ^2J_{HD}}{6} \quad (2)$$

where $^1J_{HD}$ is the coupling in the bound dihydrogen ligand, $^{2c}J^*_{HD}$ represents the two bond coupling between a *cis* hydride and the dihydrogen ligand, $^{2t}J^*_{HD}$ represents the two bond coupling between a *trans* hydride and the dihydrogen ligand, and the coupling between two adjacent hydride ligands is designated as $^2J_{HD}$. In the case of IrH$_4$ (**A**) J_{obs} is an average of three types of H−D interactions (illustrated in Chart 3, bottom) and can be interpreted using the equation

$$J_{obs} = \frac{^{2t}J_{HD} + 2^{2c}J_{HD} + 2^{2t-oid}J_{HD} + ^{2c-oid}J_{HD}}{6} \quad (3)$$

(19) Gutiérrez-Puebla, E.; Monge, A.; Paneque, M.; Poveda, M. L.; Taboada, S.; Trujillo, M.; Carmona, E. *J. Am. Chem. Soc.* **1999**, *121*, 346–354.

(20) The inability of T_1(min) alone to assign a definitive structure to polyhydride molecules has been discussed previously, see: Luo, X.-L.; Crabtree, R. H. *J. Am. Chem. Soc.* **1990**, *112*, 4813–4821.

(21) Gross, C. L.; Girolami, G. S. *Organometallics* **2007**, *26*, 1658–1664.

where $^{2t}J_{HD}$ is the two bond coupling between two *exo* hydrides, $^{2c}J_{HD}$ represents the two bond coupling between an *exo* hydride and an adjacent *endo* hydride, $^{2t\text{-}oid}J_{HD}$ represents the two bond coupling between an *exo* hydride and a nonadjacent *endo* hydride, and the coupling between two *endo* hydrides is designated as $^{2c\text{-}oid}J_{HD}$. (A hydride with one adjacent hydride is defined as *exo* and a hydride with two adjacent hydrides is defined as *endo*.)

Since the signals from all isotopomeric species in both **1** and **2** were coincident in the $^1H\{^{31}P\}$ NMR spectra, observation of individual couplings were not possible, nor was it possible to assess the affinity for D over H to occupy a particular hydridic site in any of the proposed structures.[22] On the basis of the minimal isotope effects on the chemical shift, we assume that the deuteration of the various hydridic positions in the complex is statistical.[23] All two-bond H−D couplings can be estimated as ± 1 Hz.[24] The validity of this assumption is supported by observations of $^2J_{cis\text{HH}}$ and $^2J_{trans\text{HD}}$ in various isotopomers of (POCOP)IrH_3^- Na^+. The absolute values of the H−D couplings are < 1 Hz, and it is likely that some of these couplings are opposite in sign.[24] Thus J_{obs} values of 3.6 and 4.4 Hz for **1** and **2**, respectively, correspond to values of $J_{HD} = 22 \pm 5$ Hz for **1** and $J_{HD} = 26 \pm 5$ Hz for **2**. Using the relationship developed by Heinekey and coworkers (eq 4), these couplings correspond to a dihydrogen ligand of $r_{HH} = 1.06 \pm 0.11$ Å for complex **1** and $r_{HH} = 0.97 \pm 0.09$ Å for complex **2**.[13b,25] Utilizing the assumptions outlined above, the observed H−D couplings are inconsistent with an assignment of only well-defined tetrahydride structures for either **1** or **2** in solution at or near ambient temperature. An expected J_{obs} of 0.5 Hz results when this method is used in conjunction with atom positions obtained by neutron diffraction data from complex **1**.

$$r_{HH} = 0.74 - 0.494 \times \ln\left(\frac{16.1447 - \sqrt{260.65 - 4(1 + 0.32895(J_{HD}))}}{2}\right) \quad (4)$$

Computational Studies. The potential energy surfaces for **1** and **2** are remarkably flat with respect to motion of H atoms around the Ir center in the meridional plane. The geometry optimizations on **1** located three minima and two TS's connecting them. The tetrahydride **1A** is lowest in energy but the *trans* species **1C** is computed to be less than 1 kcal/mol higher; the *cis* species **1B** is approximately 2 kcal/mol above **1A**. The differences between the minima appear to increase slightly on the enthalpy (*H*) and free energy (*G*) surfaces. The potential energy barriers for interconversion of minima **1A** and **1C** or **1B** are 1.4 and 3.3 kcal/mol, respectively. The statistical mechanical treatment of thermal energy contributions seemingly flattens the energy surface even further and finds the free energy of **1C** (1.41 kcal/mol) equal to that of the TS for its formation from **1A** (1.40 kcal/mol). Overall, the potential and free energies computed for **1** clearly indicate facile interconversion of isomers with tetrahydride **1A** favored. The dihydrogen internuclear distances in **1B** and **1C** are fairly short, $r_2 = 0.932$ Å and $r_3 = 0.890$ Å, respectively; the corresponding "short" internuclear distance (r_2) in **1A** is computed at 1.691 Å, about 0.2 Å longer than the distance in **1** determined by neutron diffraction. When the geometry of **1** is optimized with *cis* H−H distances fixed at the value of the neutron-diffraction structure ($r_2 = 1.49$ Å), the energy of the resulting structure is only 0.82 kcal/mol above that of fully relaxed **1A** ($r_2 = 1.69$ Å) and 0.20 kcal/mol above **1C** ($r_2 = 0.93$ Å).

Energy differences for the potential structures for **2** are even less than those just discussed for **1**. The tetrahydride **2A** is again predicted to be the most stable structure. The two dihydrogen structures (**2B** and **2C**) are isoenergetic on the potential energy surface but **2B** may be favored in free energy. Again, the enthalpy and free energy of the TS for the formation of the *cis* dihydrogen species is computed slightly less than the energy of the minimum (**2C**). However, all energy differences are of the order of 1 kcal/mol (or less), seriously testing the overall accuracy of the computational models employed.

Relative to the gas phase results (Table 5), the effects of a solvent, polar or non-polar (Table 6), on the H−H distances are consistently small (< 0.05 Å). However, the *cis* dihydrogen species **1B** and **2B** have small permanent dipole moments (gas phase values are 0.85 D for **1B** and 2.0 D for **2B**) and are hence favored preferentially by a solvent possessing even a modest dielectric constant such as cyclohexane. The calculations indicate that for **1**, the order of isomer stability remains **1A** < **1C** < **1B** in cyclohexane, but **1B** and **1C** are found to be isoenergetic in THF solvent and only about 1.7 kcal/mol higher in energy than **1A**. For **2**, the larger dipole moment of **2B** and the inherently smaller energy separation among the isomers combine to make **2B** the preferred structure in solution, 0.5−1.0 kcal/mol below tetrahydride **2A**.

In the idealized gas phase, which in the absence of crystal packing effects probably best approximates the neutron structure acquisition conditions, the tetrahydrides **1A** and **2A** represent the favored structures at zero (potential energy; potential plus zero-point energies) or finite (enthalpy, free energy) temperature.

Calculated and Experimental Ir−H Stretching Frequencies. The first characterized H_2 complex was detected based on its unique IR spectrum.[26] A complex containing a well-defined H_2 ligand will display a broad, weak intensity IR band corresponding to ν_{HH} which is shifted to lower wavenumber in the D_2 isotopomer of the complex. Most importantly, in the HD isotopomer, the observed band will come in between the H_2 and D_2 bands, as opposed to a mixture of the two bands as would be expected for a complex containing two hydride ligands. An excellent example of this has been reported by Upmacis and co-workers.[27] This analysis becomes ruefully complicated if the complex

(22) This eliminates the usefulness of correction factors which would account for preferential occupation of one isotope in a particular hydridic site. For a discussion of these correction factors and demonstration of how they would be applied to eqs 1−3, see: Oldham, W. J., Jr.; Hinkle, A. S.; Heinekey, D. M. *J. Am. Chem. Soc.* **1997**, *119*, 11028–11036.

(23) We do not observe a temperature dependence on the position of the hydridic signal in partially deuterated samples, indicating there is no preference for D to occupy a particular site in the molecule.

(24) Gründemann, S.; Limbach, H.-H.; Buntkowsky, G.; Sabo-Etienne, S.; Chaudret, B. *J. Phys. Chem. A* **1999**, *103*, 4752–4754.

(25) This analysis does not attempt to differentiate between the *cis* or *trans* isomers of **Ir(H$_2$)H$_2$**.

(26) Kubas, G. J. *Acc. Chem. Res.* **1988**, *21*, 120–128.

(27) Upmacis, R. K.; Poliakoff, M.; Turner, J. J. *J. Am. Chem. Soc.* **1986**, *108*, 3645–3651.

potentially contains both hydride and dihydrogen ligands or an elongated dihydrogen ligand.[28] This is the case for complexes **1** and **2** in the present work, where facile incorporation of D into C−H bonds on the ligand further hinder definitive assignment of IR bands in the isotopomers.[5d] Nevertheless, DFT calculations of the IR spectra of the several geometries of **1** which we have considered do offer significant structural insight. In particular, in combination with the experimental data, the calculations can be used to rule out the possibility that at or near ambient temperatures, complex **1** could be well represented as a simple dihydrogen complex with a short H−H distance (i.e., structures **B** or **C**).

The experimental IR spectrum of **1** (Figure 2) in the Ir−H stretch region spans about 250 cm^{-1} and shows the strongest absorption peak (in cyclopentane solution) at 1884 cm^{-1}, a medium strength absorption peaking at 2076 cm^{-1}, and a weak absorption peak at 2127 cm^{-1}. The spectrum of **1** in KBr appears similar in terms of the number of distinct absorption bands (three), their frequencies (1902, 2073, and 2127 cm^{-1}, respectively), and dominant relative intensities (strong, medium, and weak), suggesting that the absorbing species have similar conformations in both phases.

The calculated Ir−H stretch region (in simulated cyclohexane solvent and the harmonic oscillator approximation) of **1** contains the expected four frequencies (Figure 4) and spans a range of 250 cm^{-1} for **1A**, but no less than 650 cm^{-1} and 850 cm^{-1} for **1C** and **1B**, respectively. The predicted intensities for **1C** do not match the experimental observations, since a virtually nonexistent medium energy peak flanked by strong absorption on both the high and low energy sides is predicted. The intensity pattern predicted for **1B** is also inconsistent with experimental observations, even if one assumes that it is the low energy, weak absorption predicted at 1834 cm^{-1} that is not observed in the experiments. The intensity pattern for **1A**, however, is in agreement with experimental observations if one assumes that ν_3 (2158 cm^{-1}) is either not observed as a separate feature or is contributing with ν_4 (2190 cm^{-1}) to the weak, high energy peak observed experimentally at 2127 cm^{-1}. The computed harmonic frequencies for **1A** are only 2−3% larger than the experimental observations; in fact, a uniform red-shift of about 50 cm^{-1} brings the computed and experimental frequencies in near coincidence. A normal mode calculation on a nonequilibrium structure, in which the *cis* H−H distance had been constrained to the neutron diffraction value of 1.488 Å (all remaining parameters were relaxed), resulted in only modest changes in the computed Ir−H frequencies (see Supporting Information).

The high frequency mode (ν_4) has substantial dihydrogen H−H stretch character in **1B** and **1C**, and its large numerical value, which places it well outside the Ir−H frequency region, could partly be a reflection of a systematic underestimation of dihydrogen H−H distances by the B3LYP calculations as well as use of the harmonic approximation. Indeed, the anharmonicity corrections computed for ν_4 in **1B** and **1C** are substantial (Table 7: 339 cm^{-1} for **1−H-C**, 569 cm^{-1} for **1−H-B**). However, even when approximate anharmonicity corrections have been included, the calculated Ir−H stretch region (Table 7) spans a range of 225 cm^{-1} for **1A**, but 400−475 cm^{-1} for **1C** and **1B**; the experimentally observed frequencies span a range of 250 cm^{-1} (Figure 2). Also, the individual frequencies for **1A**, approximately corrected for anharmonicity, do match the experimental spectrum quite well.

(28) Kubas, G. J. *Metal Dihydrogen and σ-Bond Complexes*; Kluwer Academic/Plenum Publishers: New York, 2001; pp 248−258.

Conclusions

Neutron diffraction data indicate a compressed dihydride structure for **1** ($r_{HH} \approx 1.49$ Å), while the J_{HD} couplings obtained from NMR spectroscopy studies suggest a dihydrogen/dihydride structure. While the diffraction study pertains to the solid state and the NMR data were obtained in solution, it does not seem likely that solid state packing effects could strongly favor either of these structures. While solvent effects might seem a more likely source of the discrepancy, the fact that major variations in solvent had little effect on the values of J_{obs} seems to argue strongly against the importance of solvent effects. Moreover, the solution and solid phase (KBr) IR spectra of **1** are essentially identical. Calculations strongly indicate that for a solution of **1** in alkane solvent, the IR absorbing conformer is structurally very similar to the tetrahydride, **1A**.

Electronic structure calculations for complex **1** in the gas phase and in solution (cyclohexane or THF simulated) indicate that the global minimum in either case is a tetrahydride structure; this would further argue against crystal packing effects being responsible for the structures afforded by the diffraction studies. For **2**, the calculations indicate a tetrahydride structure as favored in the gas phase; in solution, the calculations predict that the *cis*-H_2 dihydrogen/dihydride conformer is favored. Calculations of vibrational Ir−H frequencies and intensities are most consistent with a tetrahydride structure for **1**. The coupling constant results thus appear incongruous, but the high values of J_{HD} are unambiguous and do not appear to be consistent with the sole presence of simple tetrahydride structures.

The computational studies of **1** (and **2**) assist in resolving this apparent discrepancy between crystallographic and spectroscopic data. The computed energy differences separating the various structural minima are probably too small to be taken entirely at face value. The outstanding feature of the calculated surfaces, however, is the presence of nearly isoenergetic minima with both tetrahydride and dihydride/dihydrogen character, as well as exceptionally low barriers to structural interconversion. The extremely flat potential energy surface computed allows several explanations that can reconcile these apparently incompatible experimental results. These explanations are not entirely independent but can be reasonably categorized as follows.

(1) Perhaps the simplest argument to reconcile the computational, diffraction, and NMR results is based simply on Boltzmann populations. The NMR data are necessarily obtained at temperatures greater than 100 K as applied in the diffraction studies. The higher temperatures would allow a significant population of the low-energy dihydrogen/dihydride isomers, which might contribute substantially to the high values of J_{obs}. The independence of the NMR spectroscopy data

on temperature, however, indicates that these energies are nearly identical.

(2) Even in the absence of a significant population of any state with well-defined dihydrogen-complex-like character, Lluch and co-workers[29] have shown that excited vibrational states, and in particular the $\nu = 1$ state, of a "dihydride" energy minimum can have predominantly dihydrogen character. (In that work, a J_{HD} value of 22.3 Hz was calculated for the $\nu = 1$ state versus 6.0 Hz for the vibrational ground state.) In view of the exceptional flatness of the energy surfaces calculated for **1** and **2**, a significant population of such states seems quite plausible in the present case. Nuclear motions couple the **1A** and **1C** conformations, and the *cis*-hydrogens should be considered as moving in an asymmetric double-well potential.

(3) Finally, as has also been emphasized by Lluch and co-workers[29] the displacement in the vibrational ground state of a dihydride complex can be quite substantial and have significant dihydrogen character. Simple application of analytic harmonic oscillator formulas indicate that an H_2 oscillator of frequency 2,000 cm^{-1} has a rms displacement ($\langle x^2 \rangle^{1/2}$) of approximately 0.1 Å, indicating that a large number of different geometries will be sampled by the *cis*-hydrogens in **1**, even at low temperatures. A high degree of dihydrogen/dihydride (and tetrahydride) character in a macroscopic sample of compressed dihydride (PCP)IrH_4 molecules results.

Qualitatively, our spectroscopic, diffraction, and computational data suggest, when taken together, that complexes **1** and **2** are not optimally characterized in terms of individual well-defined structures. Rather, extensive nuclear motions on the exceptionally flat energy surfaces offer the simplest and most appropriate descriptors for these molecules.

Experimental Section

General Considerations. All manipulations were carried out under an atmosphere of argon in a glovebox (Vacuum Atmospheres) or using Schlenk techniques. THF-d_8 was vacuum transferred from sodium metal/benzophenone. Cyclopentane, toluene-d_8, and MeCy-d_{14} were vacuum transferred from Na/K alloy. CD_2Cl_2 and CD_5F were vacuum transferred from CaH_2. Acetone-d_6 was vacuum transferred from activated 4 Å molecular sieves.

Solution NMR spectra were collected at room temperature unless otherwise specified using Bruker AV500 and DRX500 spectrometers. ^1H NMR spectra were referenced to residual solvent signals, and shifts are reported in parts per million (ppm) downfield of tetramethylsilane. $^{31}P\{^1H\}$ NMR spectra were referenced to an external H_3PO_4 (85%) sample set to 0 ppm. Relaxation rate (T_1) experiments were conducted using a saturation recovery pulse sequence ($180-\tau-90$). Temperature measurements for variable temperature experiments were calibrated using a sample of neat methanol. Infrared spectra were recorded on a Bruker Optics Tensor27 FT-IR spectrometer at room temperature. Complexes (POCOP)IrH_3^- Na^+ (PCP)IrH_4 and (POCOP)IrH_4 were synthesized according to literature procedures.[2a,g]

Neutron Diffraction Study of Complex 1. Neutron diffraction data were obtained at the Intense Pulsed Neutron Source (IPNS) at Argonne National Laboratory using the time-of-flight Laue single crystal diffractometer (SCD).[30] At the IPNS, pulses of protons are accelerated into a heavy-element target 30 times a second to produce pulses of neutrons by the spallation process. Because of the pulsed nature of the source, neutron wavelengths are determined by time-of-flight based on the de Broglie equation $\lambda = (h/m)\cdot(t/l)$, where h is Planck's constant, m is the neutron mass, and t is the time-of-flight for a flight path l, so that the entire thermal spectrum of neutrons can be used. With position-sensitive area detectors and a range of neutron wavelengths, a solid volume of reciprocal space is sampled with each stationary orientation of the sample and the detectors. The SCD has two ^{6}Li-glass scintillation position-sensitive area detectors, each with active areas of 15×15 cm^2 and a spatial resolution of < 1.5 mm. One of the detectors is centered at a scattering angle of 75° and a crystal-to-detector distance of 23 cm, and the second detector is at 120° and 18 cm. Details of the data collection and analysis procedures have been published previously.[31]

A crystal of complex **1** with approximate dimensions of $2 \times 1 \times 1$ mm^3 was covered in a fluorocarbon grease in a glovebag, wrapped in aluminum foil and glued to an aluminum pin which was mounted on the cold stage of a closed-cycle helium refrigerator operating at 100 ± 0.1 K. For each setting of the diffractometer angles, data were stored in three-dimensional histogram form with coordinates x, y, t corresponding to horizontal and vertical detector positions and the time-of-flight, respectively. An auto-indexing algorithm[32] was used to obtain an initial orientation matrix from the peaks in one histogram. For intensity data collection, 19 diffractometer settings were used to obtain at least one unique quadrant of reciprocal space plus some duplicate data.

Refinement. Bragg reflections were integrated about their predicted location and were corrected for the Lorentz factor, the incident spectrum, and the detector efficiency. A wavelength-dependent spherical absorption correction was applied using cross sections from Sears[33] for the non-hydrogen atoms and from Howard and co-workers[34] for the hydrogen atoms. Symmetry-related reflections were not averaged since different extinction factors are applicable to reflections measured at different wavelengths. The GSAS software package was used for structural analysis.[35] The atomic positions of the X-ray diffraction structure were used as a starting point in the refinement (see the Supporting Information). The refinement was based on F^2 using 3586 reflections with a minimum d-spacing of 0.7 Å. Weights were assigned as $w(F_o^2) = 1/[(\sigma(F_o^2) + (0.005F_o^2)^2]^2$ where $\sigma^2(F_o^2)$ is the variance based on counting statistics. In the final refinement, all atoms, except H(4), which lies upon a 2-fold axis, were refined with anisotropic displacement parameters. Two twin domains were refined, the merohedral twin component corresponding to the transformation (k, h, $-l$) refined to 44% of the structure, and an inversion twin component ($-h$, $-k$, $-l$) refined to 36%. The refinement used 372 variables and converged to $R_w(F) = 0.072$ and $R(F) = 0.124$. Data collection and refinement parameters are summarized in the Supporting Information.

(29) Gelabert, R.; Moreno, M.; Lluch, J. M.; Lledós, A.; Heinekey, D. M. *J. Am. Chem. Soc.* **2005**, *127*, 5632–5640.

(30) (a) Schultz, A. J.; Srinivasan, K.; Teller, R. G.; Williams, J. M.; Lukehart, C. M. *J. Am. Chem. Soc.* **1984**, *106*, 999–1003. (b) Schultz, A. J. *Trans. Am. Crystallogr. Assoc.* **1987**, *23*, 61–69.

(31) Schultz, A. J.; Van Derveer, D. G.; Parker, D. W.; Baldwin, J. E. *Acta Crystallogr., Sect. C* **1990**, *46*, 276–279.

(32) Jacobson, R. A. *J. Appl. Crystallogr.* **1986**, *19*, 283–286.

(33) Sears, V. F. In *Methods of Experimental Physics*; Sköld, K., Price, D. L., Eds.; Academic Press: Orlando, FL, 1986; Vol. *23*, Neutron Scattering, Part A, pp 521−550.

(34) Howard, J. A. K.; Johnson, O.; Schultz, A. J.; Stringer, A. M. *J. Appl. Crystallogr.* **1987**, *20*, 120–122.

(35) Larson, A. C.; Von Dreele, R. B. *General Structure Analysis System-GSAS*; Los Alamos National Laboratory: Los Alamos, NM, 2000.

Computational Details. Most calculations used the SDD-model 60-electron relativistic effective core potential (ECP) and corresponding valence basis set (6s5p3d) for the Ir atom;[36] all-electron, full double-ζ plus polarization function basis sets on the second and third row elements C, O, and P (Dunning−Huzinaga D95(d));[37] a triple-ζ plus polarization 311G(p) basis set for the four hydridic H atoms;[38] and a double-ζ quality 21G basis set for all hydrogen atoms in the pincer ligands.[39] Most calculations were performed on the actual species used in the experiments, that is, the ^{t}Bu groups were kept on the phosphorus atoms in the PCP and POCOP ligands. All stationary points located on the potential energy surfaces were characterized by normal-mode analysis as minima or transition states. The (unscaled) vibrational frequencies formed the basis for the calculation of vibrational zero-point energy (ZPE) corrections. Standard thermodynamic corrections (based on the harmonic oscillator/rigid rotor approximations and ideal gas behavior) were made to convert from potential energies (ΔE, $\Delta E^{\ddagger}$; no ΔZPE) to (standard) enthalpies ($\Delta H°$, $\Delta H°^{\ddagger}$; ΔZPE included, $T = 298$ K) and Gibbs free energies ($\Delta G°$, $\Delta G°^{\ddagger}$; $T = 298$ K, $P = 1$ atm for all species).[40]

General solvent effects were incorporated with the CPCM self-consistent reaction field model,[41] using default parameters provided in Gaussian 03 for cyclohexane and THF solvents. Free energies for species in solution were estimated at $P = 1$ atm, $T = 298$ K by adding the thermal free energy corrections from gas phase calculations to the total potential energies obtained from the calculations including solvent effects. All computational work was performed with the GAUSSIAN03[42] software package.

Acknowledgment. Low-temperature single-crystal neutron data were collected at the Intense Pulsed Neutron Source Division (IPNS) of Argonne National Laboratory (ANL). The authors would like to thank Arthur J. Schultz and John A. Cowan for their help in collecting, processing, and refining the neutron data. Research at the University of Washington was supported by the U.S. Department of Energy as part of the Center of Excellence for Chemical Hydrogen Storage. Partial support was provided by the NSF (CHE-454683 to D.M.H., and CHE-0719307 to A.S.G.).

Supporting Information Available: Detailed tables of NMR spectroscopy data; IR spectra of **1**; CIF files for **1**, data collection, refinement parameters, bond distances and angles obtained from neutron and X-ray diffraction data of **1**; detailed results from computational studies of **1** and **2** including calculated IR frequencies: complete reference 42; gas phase geometries and energetics for **1** and **2** (B3LYP). This material is available free of charge via the Internet at http://pubs.acs.org.

(36) Andrae, D.; Häussermann, U.; Dolg, M.; Stoll, H.; Preuss, H. *Theor. Chim. Acta* **1990**, *77*, 123–141.
(37) Dunning, T. H.; Hay, P. J. In *Modern Theoretical Chemistry*; Schaefer, H. F., III, Ed.; Plenum: New York, 1976; pp 1−28.
(38) Krishnan, R.; Binkley, J. S.; Seeger, R.; Pople, J. A. *J. Chem. Phys.* **1980**, *72*, 650–654.
(39) Binkley, J. S.; Pople, J. A.; Hehre, W. J. *J. Am. Chem. Soc.* **1980**, *102*, 939–947.
(40) McQuarrie, D. A. *Statistical Thermodynamics*; Harper & Row: New York, 1973.
(41) Cossi, M.; Barone, V. *J. Phys. Chem. A* **1998**, *102*, 1995–2001.
(42) Frisch, M. J. et al. *Gaussian 03*, Revision C.02; Gaussian, Inc.: Pittsburgh, PA, 2003. See the Supporting Information for the complete reference.